Exploring Airfoil Table Generation using XFOIL and OVERFLOW

Kristen Kallstrom
Aerospace Engineer
NASA Ames Research Center
Moffett Field, CA, 94035

ABSTRACT

The rotorcraft design process is a continuously evolving field of research that incorporates a number of software programs. An accurate airfoil table is critical in the design and testing process for rotorcraft. With multiple flow solvers available and flow conditions of multirotor UAM vehicles potentially covering a wide range of Reynolds and Mach numbers, a documented approach for developing airfoil tables is needed. Using benchmark data from legacy airfoil tables and wind tunnel tests for comparison, simulations for a comprehensive test matrix could guide rotorcraft design engineers in generating their own airfoil tables using the XFOIL and OVERFLOW solvers. The motivation for this study is to investigate flow solver features to develop a best practices document for airfoil table generation. The study uses the OVERFLOW and XFOIL flow solvers, coupled with the airfoil table generator AFTGen, to analyze three airfoils for a specific Reynolds numbers flow regime and provide details on how well each flow solver performs within a specific angle of attack range, Mach number range, Reynolds number range, and in different flow conditions, such as turbulent and transitional flow. OVERFLOW analyses in AFTGen for fully turbulent and transition flow are compared with XFOIL results and experimental test data for the section lift, section drag, and pressure coefficients. XFOIL ultimately yields results that are accurate within the linear angle of attack range and below a Mach number of 0.4 but tends to overpredict lift and underpredict drag unless the flow is in the compressible regime. XFOIL cannot accurately model stall and post-stall conditions due to the nature of the solver. This is evident in nearly every case run with XFOIL, where the linear range is usually predicted acceptably and the lift coefficient is overpredicted as the stall angle of attack is approached (with the exception being the generally poor correlation with most of the SSC-A09 cases). OVERFLOW is limited at low Mach numbers, and appears to perform best at Mach numbers of 0.4 and above. The exploration of airfoil table generation using XFOIL and OVERFLOW yielded moderately successful results for the NACA 0012 airfoil, reasonably good results for the RC(4)-10 airfoil, and less accurate results for the SSC-A09 airfoil.

NOTATION

c	airfoil chord length
c_d	section drag coefficient
c_l	section lift coefficient
c_m	section moment coefficient
c_p	pressure coefficient
M	Mach number
p	pressure, atm/psia
Re	Reynolds number
Re/M	Reynolds Mach proportionality constant
T	static temperature, R°
$y+$	spacing of grid normal to airfoil surface
α	angle of attack, deg
η	number of normal grid points
ξ	number of periodic grid points

INTRODUCTION

The rotorcraft community continues to push for Urban Air Mobility (UAM) technology growth; in particular, electric Vertical Take-Off and Landing (eVTOL) vehicles are being developed for personal flight, air taxi purposes, and emergency applications. Over the past few decades, computer technology has transformed the way engineering can be accomplished by enabling increasingly rapid simulations that greatly expedite the aircraft design process and by providing pre-test predictions for wind tunnel and flight tests of air vehicles, especially multirotor UAM aircraft. Rotorcraft conceptual design tools typically incorporate lower-fidelity aerodynamics to represent the rotor and will often use look-up tables containing airfoil lift, drag, and moment coefficients.

Airfoil geometries are selected for rotor blade and wing design based on their aerodynamic characteristics, structural properties, and overall manufacturability. Characteristics such as thickness and camber define an airfoil's geometry and contribute to its aerodynamic performance. An airfoil table provides the sectional lift (c_l), sectional drag (c_d), and sectional moment (c_m) coefficients for wing or blade cross-sectional profiles (or

geometries) as a function of angle of attack (α) and Mach number (M). Together, these values can provide an approximation of an entire wing or blade's overall aerodynamic characteristics. The angle of attack range spans ±180 deg for multiple Mach numbers. These coefficients are determined by integrating pressure and shear stress distributions over the surface of an airfoil, and breaking these resultant forces down into lift, drag, and moment components [Ref. 1]. Airfoil tables can be established from wind tunnel experiments, simulations, or a combination of both, and are typically formatted in .c81 format. A full c81-formatted table provides the lift coefficients first, drag coefficients second, and finally the moment coefficients as a function of α and M. Figure 1 shows a partial .c81 table, with a small section of the lift coefficient at negative angles of attack for Mach numbers from 0 through 1.

```
NACA 0012                   11391165 947
        0.    .20   .30   .40   .50   .60   .7   .75   .8
        .9    1.
-180.  0.    0.    0.    0.    0.    0.    0.    0.    0.
        0.    0.
-172.5 .78   .78   .78   .78   .78   .78   .78   .78   .78
        .78   .78
-161.  .62   .62   .62   .62   .62   .62   .62   .62   .62
        .62   .62
-147.  1.    1.    1.    1.    1.    1.    1.    1.    1.
        1.    1.
-129.  1.    1.    1.    1.    1.    1.    1.    1.    1.
        1.    1.
-49.   -1.18 -1.18 -1.18 -1.18 -1.18 -1.18 -1.18 -1.18 -1.18
        -1.18 -1.18
-39.   -1.18 -1.18 -1.18 -1.18 -1.18 -1.18 -1.18 -1.18 -1.18
        -1.18 -1.18
-21.   -.8   -.8   -.81  -.83  -.85  -.85  -.85  -.71  -.68
        -.64  -.64
-16.5  -1.007 -1.007 -.944 -.96 -.965 -.965 -.965 -.795 -.76
        -.7   -.7
-15.   -1.19 -1.19 -1.09 -1.055 -.99 -.98  -.98  -.83  -.79
        -.72  -.72
```

Figure 1. Legacy NACA 0012 .c81 airfoil table – partial table.

The header of the table depicts the airfoil name, with the number sequence identifying the number of Mach and alpha values for the section lift coefficient, section drag coefficients, and section moment coefficient. Table 1 describes the heading numbers with respect to each of the aerodynamic coefficients.

Table 1. Breakdown of .c81 header description.

NACA 0012	11391165 947
11	number of Mach points for the section c_l
39	number of α points for the section c_l
11	number of Mach points for the section c_d
65	number of α points for the section c_d
9	number of Mach points for the section c_m
47	number of α points for the section c_m

Airfoil tables are used by comprehensive rotorcraft analysis codes as well as some hybrid computational fluid dynamics (CFD) simulations, so a full range of angle of attack data is desired to provide aerodynamic data that encompasses an entire rotor revolution.

The motivation for this study is to investigate features of the XFOIL and OVERFLOW flow solvers, coupled with AFTGen. The features investigated include the number of trailing edge points and clustering iterations, as well as a study of the effect of leading edge coordinate point density. The following sections will discuss the NACA 0012, RC(4)-10, and SSC-A09 airfoils, provide information on the flow solvers and the airfoil table generator tool, and compare the experimental lift, drag, and pressure coefficients with XFOIL and OVERFLOW calculations. Comparison of simulated results with well referenced historical data for comparison will provide a suitable foundation for the development of airfoil table best practices.

APPROACH

The NACA 0012, RC(4)-10, and SSC-A09 airfoils were selected for analysis using the XFOIL and OVERFLOW solvers based on existing, well known experimental data. The airfoil geometries were smoothed using a spline fit to improve grid resolution as the leading edge. Subsequent trailing edge point and grid clustering iterations studies were performed to investigate some of the features of AFTGen, using the OVERFLOW solver. The following section provides more detail on these airfoils as well as the approaches used to solve for the aerodynamic coefficients compared against experimental wind tunnel test data.

Legacy Airfoil Tables

Legacy airfoil tables are widely used and circulated within the rotorcraft community. Legacy airfoils include NACA 4-, 5-, and 6-series airfoils, which have served as benchmarks for checking experimental test setups in wind tunnels and simulation results [Ref. 2]. However, one challenge is that occasionally, the original source of an airfoil table being circulated is not known, and therefore the fidelity of the values is uncertain. In addition, some circulated tables are a composite of multiple sources, including both measured and computed values.

Airfoil Selection

The airfoils selected for this study are relevant because there is a large amount of experimental data that can be used to evaluate simulation results, and additionally, the geometries are publicly available for use. Having accessible, validated airfoil tables for use in pre-test predictions, for both CFD and comprehensive analysis applications, will support design and analysis efforts of next-generation rotary wing concepts.

The NACA 0012 was selected as a benchmark airfoil because of the wealth of data available for reference,

dating from as early as 1939. In 1987, McCroskey [Ref. 3] asserts that data collected by Harris [Ref. 4] in 1981 provides the most reliable results with respect to lift and drag characteristics. The full .c81 table referenced in this report was developed by Davis [Ref. 5] using a rotorcraft flight simulation program. The 0012 airfoil is uncambered with a maximum thickness of 12% of the chord length. Figure 2 depicts the profile of the NACA 0012 airfoil.
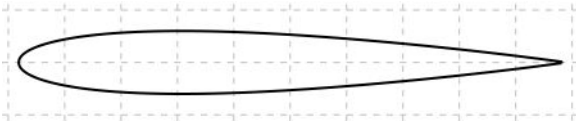

Figure 2. NACA 0012 airfoil geometry as generated in AFTGen.

The RC(4)-10 airfoil is one of a series designed at NASA's Langley Research Center to advance airfoil concepts that optimize rotorcraft performance. In 1990, Noonan [Ref. 6] determined the sectional lift, drag, and moment coefficients for the RC(4)-10 and the RC(5)-10 airfoils and compared them against the baseline VR-7 airfoil. Wind tunnel testing was completed in NASA Langley's 6-by 28-Inch Transonic Wind Tunnel and the Low-Turbulence Pressure Tunnel for Mach numbers from 0.3 - 0.84 and 0.10 to 0.44, respectively. This test does not include corrections for wind tunnel sidewall boundary effects. For this reason, data collected in this tunnel tends to show a reduced maximum lift coefficient, by around 0.09, particularly at Mach 0.34. The RC(4)-10 airfoil profile is depicted in Figure 3.
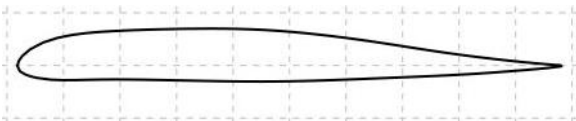
Figure 3. The RC(4)-10 airfoil as generated in AFTGen.

The SSC-A09 airfoil is a "third generation" airfoil developed by Sikorsky Aircraft alongside other airfoils intending to improve upon earlier SC airfoils. In 1984, Flemming [Ref. 7] discusses a NASA Ames Research Center and Sikorsky Aircraft jointly supported test program with the intention of reducing the drag divergence Mach number by a minimum of 0.03. The SSC-A09 was tested alongside a number of other transonic airfoils in NASA Ames's 11-Foot Transonic Wind Tunnel at Mach numbers from 0.3 to 1.07. Stagnation pressure was 1.0 and 1.4 atmospheres, with an average stagnation temperature of approximately 530 deg Rankine. The SSC-A09 profile has a maximum camber of 1.2% at 17.2% chord, with a maximum thickness of 9% at 37.7% chord. Figure 4 shows the SSC-A09 airfoil profile.
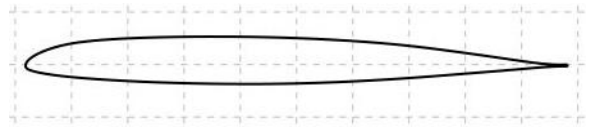
Figure 4. SSC-A09 airfoil profile as generated in AFTGen.

Computational Tools

Aerodynamic coefficients were generated using AFTGen for ±20 deg angle of attack from Mach numbers ranging from 0 to 1 for the NACA 0012, 0.3 to 0.85 for the SSC-A09, and 0.37 to 0.9 for the RC(4)-10, with the Mach number and Reynolds numbers selected based on the Mach and Reynolds number ranges available in the experimental test data. AFTGen is a software tool developed by Sukra-Helitek that provides a GUI interface for XFOIL, MSES, ARC2D, UNS2D, and OVERFLOW [Ref. 8]. AFTGen provides a user-friendly interface that enables a range of low-, mid-, and high-fidelity flow solvers to analyze a single-element airfoil using a built-in grid generator. AFTGen also features a C81blender module that allows the user to combine partially populated airfoil tables in order of preference, resulting in a single airfoil table spanning full angle of attack and Mach values. The flow solvers of interest in this study are XFOIL and OVERFLOW as they represent low-fidelity and high-fidelity codes.

XFOIL, developed by Mark Drela at MIT, is a reliable tool for generating airfoil tables quickly, and is a valuable design tool for subcritical airfoils in both viscous and inviscid flows at low Reynolds numbers [Ref. 9]. The XFOIL code focuses on determining two-dimensional boundary layer aerodynamics for both inviscid and viscous flows. XFOIL inputs include chord-normalized airfoil coordinates, flow conditions (viscous flow parameters, Reynolds number, Mach number, etc.), and the desired angle of attack range. Within seconds, the code produces an airfoil polar output file containing data on the pressure, lift, drag, and moment coefficients, in addition to the location of boundary layer transition from laminar to turbulent flow on the upper and lower surfaces of the airfoil. 2D performance calculations are accomplished via a mixture of numerical methods that allow XFOIL to accurately capture boundary layer aerodynamics. XFOIL's computational methods, while ensuring quick calculations, are not valid for transonic and sonic flows, which can limit its use for helicopter rotor flow conditions.

OVERFLOW is a high-fidelity, Reynolds-averaged Navier Stokes flow solver [Ref. 10]. Developed by Buning et al., OVERFLOW is currently used in US industry as well as within NASA. The high-fidelity OVERFLOW solver incorporates three transition models

as part of its flow numerical scheme. The Spalart-Allmaras 1-neg Coder transition model and a fully turbulent Spalart-Allmaras model are selected for simulations and compared for accuracy against established airfoil table data. XFOIL can be used to similarly identify fixed transition locations for the linear angle of attack range leading up to the maximum lift coefficient.

XFOIL Panels and OVERFLOW Grid

In this study, the XFOIL and OVERFLOW solvers will be highlighted. The panels used in XFOIL calculations are generated using the built-in airfoil paneling tool in AFTGen. XFOIL is a potential flow code that uses a panel method to represent the airfoil, with the number of panels ranging from 160 to 400 total panels for use in calculations. Increasing the number of panels results in longer computation time (from seconds to minutes) and refines panel resolution. The panel resolution was set to 400 for all XFOIL cases, to improve the code's ability to converge and accurately calculate aerodynamic coefficients. An Ncrit value of 9 was used for the NACA 0012 airfoil, with the RC(4)-10 and SSC-A09 airfoils both run in XFOIL with an NCrit value of 4.

Open trailing edge airfoil geometries were selected for analysis, although AFTGen automatically blunts and closes the trailing edge once the coordinates are imported into the program. Because the airfoils loaded into AFTGen in this study have blunt trailing edges, an O-grid topology was selected for use with the finite-difference code OVERFLOW. AFTGen's built-in grid generator tool was used to generate the O-grid, with an example shown in Figure 5, where ξ represents the number of periodic grid points and η represents the number of normal grid points.
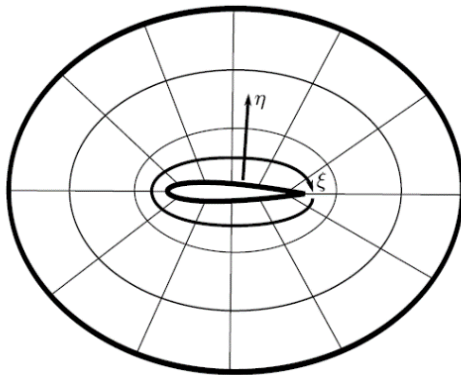

Figure 5. OVERFLOW O-grid [Ref. 8].

As multiple parameters are explored during the course of this study, standard AFTGen settings were selected for the grid. OVERFLOW simulations were run for $\xi = 201$

and $\eta = 101$. Other parameters, including the leading-edge profile, minimum points between corners, and clustering iterations are also explored, with all three traits influencing convergence.

Leading Edge Geometry Refinement

In this section, the number of coordinates points used for the initial geometry is explored, and the final grid is produced by resampling the coordinate points to produce the final grid. Coordinates for the NACA 0012 were obtained using published equations for the surface geometry, while the RC(4)-10 and SSC-A09 are only available as a limited set of coordinate points as obtained from the UIUC database [Ref. 11]. The default NACA 0012 geometry includes approximately 400 coordinate points. In contrast, the RC(4)-10 and SSC-A09 geometry obtained from the UIUC database contain 83 and 131 coordinate points, respectively. Preliminary results using the OVERFLOW solver and the UIUC default profiles resulted in a coarser gridding around the leading edge, which in turn resulted in a large discrepancy between calculations and experimental data for all of the RC(4)-10 cases. To improve this gridding around the leading edge, the leading edge of these airfoils was refined using a MATLAB code that allowed more point clustering (using a number of points specified by the user) around the leading edge using a spline fit. Figure 6 shows the leading-edge density in the default and improved coordinate file for the RC(4)-10 airfoil. Figure 7 similarly compares the default coordinates with a denser leading-edge profile for the SSC-A09 airfoil.
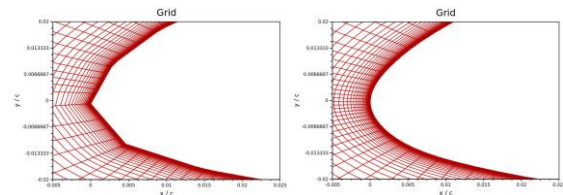

Figure 6. Close up of the leading edge of the RC(4)-10 airfoil; default coordinates (left) and the denser leading edge coordinates (right).
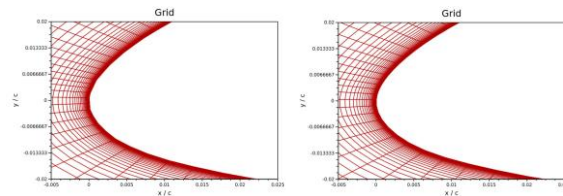

Figure 7. Close up of the leading edge of the SSC-A09 airfoil; default coordinates (left) and denser leading-edge coordinates (right).

The leading-edge points were refined for 0<= x/c <= 0.15 for both the upper and lower surface. The original (x/c, y/c) values were input into a MATLAB code which

4

interpolated point by point to increase the number of points (equally spaced) for that specified section. This approach was particularly effective for the RC(4)-10, which yielded more accurate correlation with experimental data. The discrepancies, and possible explanations for these discrepancies, with respect to the SSC-A09 results are discussed in later sections.

Trailing Edge and Clustering Iterations Study

Two secondary grid conditions of interest, the number of points across the blunt face of the trailing edge (TE) and the clustering iterations (CI), were varied to assess the impact on the OVERFLOW simulation correlation with experimental test data.

The number of trailing edge points are the number of points used along the blunt trailing edge of the geometry. The default value for these points is 3 for the OVERFLOW solver and can be increased as needed to improve refinement in this area. Increasing the trailing edge points can improve the resolution at the trailing edge, which can better resolve separated vortices and other flow phenomenon that may occur in this area. However, it should be noted that increasing the number of trailing edge points means a loss in resolution in other regions of the grid, as it counts toward the total number of periodic points used in grid generation.

AFTGen provides an option to increase the number of clustering iterations used for its grid generation. By definition, the number of clustering iterations indicates the number of total iterations used to cluster the grid points in the periodic (ξ) direction on the airfoil surface [Ref. 10]. An iterative technique is used by AFTGen that results in point clustering along the airfoil surface. Table 2 summarizes the simulation inputs for the trailing edge and clustering iterations study.

Table 2. AFTGen inputs for the trailing edge and clustering iterations studies.

| OVERFLOW	Fully Turbulent S-A Model		
Airfoil	NACA0012	RC(4)-10	SSC-A09
Re number	$5.2x10^{6*}$	$3.9x10^6$ $3.8x10^6$ $6x10^6$ $7.9x10^6$	$5.16x10^6$
M	0.3, 0.4	0.37 to 0.9	0.599
α, $\Delta1°$	$\pm8°$ to 17°	-4° to 16°	-1° to 20°
ξ, η^{**}	(201,101)	(201,101)	(201,101)
TE***,$\Delta2$	3 to 41	3 to 41	3 to 41
CI, $\Delta5K$	10K to 60K	10K to 60K	10K to 60K

* Re/M – Reynolds Mach proportionality constant
**number of points in normal and periodic direction
**number of points across blunt trailing edge face

Trailing edge cases were run in the $c_{l,max}$ range for the 0012 airfoil (8 - 17 deg angle of attack) at Mach numbers of 0.3 and 0.4 and Reynolds-Mach (*Re/M*) proportionality constant of $5.2x10^6$. For the RC(4)-10, cases were run for an angle of attack range of -4 - 16 deg for Mach numbers of 0.34, 0.37, 0.49, and 0.63 at respective Reynolds numbers of $3.9x10^6$, $3.8x10^6$, $3.8x10^6$, and $7.9x10^6$. These pairings were selected based on their correlation with experimental test data and to provide comparisons between XFOIL and OVERFLOW. The TE points included odd numbers only, with a step size of 2 points up until 41 total TE points. Figure 8 and Figure 9 show the TE point results for the 0012 at Mach number of 0.3 and 0.4.
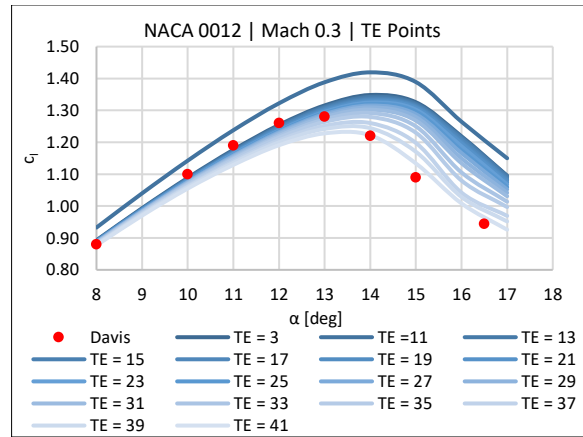

Figure 8. TE point change for the NACA 0012 at *M* = 0.3 and *Re/M* = 5.2x10⁶.
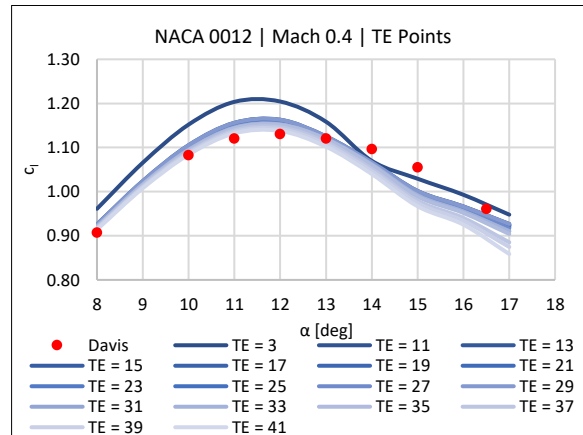
**Figure 9. TE point change for the NACA 0012 at *M* = 0.4 and *Re/M* = 5.2x10⁶.**

Increasing the number of trailing edge points for both NACA 0012 cases results in the maximum lift coefficient approaching the value in the legacy airfoil table, depicted in red. However, neither of the cases result in a close comparison with the stall region of the airfoil. The maximum lift coefficient for the Mach 0.3 case seems to occur at a higher angle of attack than seen with the

experimental test data. For the Mach 0.4 case, the correlation is marginally better, but still does not produce a result that matches the experimental data trend. This seems to be consistent with NACA 0012 results overall (discussed in later sections). Increasing beyond 11 TE points shows that the lift curve nearly converges to the same lift coefficient up to 33 TE points. Beyond this number of points, from 37 to 41, this same "convergence" trend is not seen. The increase in trailing edge point count seems to converge and show results that are nearly identical past a value of 33 TE points for the Mach 0.4 case. For subsequent NACA 0012 simulations, the trailing edge points was set to 33. A similar trailing edge study for the RC(4)-10 was completed, with results shown in Figure 10, Figure 11, and Figure 12.
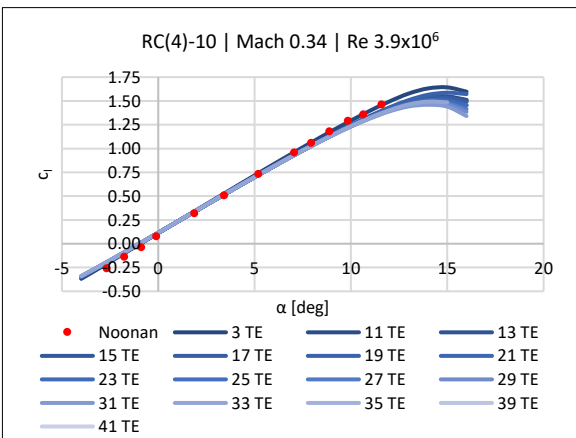
Figure 10. Lift coefficient versus angle of attack for the RC(4)-10 airfoil at $M = 0.34$ and $Re = 3.9 \times 10^6$.

For $M = 0.34$ (Fig. 10), the RC(4)-10 correlation with the Noonan experimental data does not improve – in fact, at these Mach-Reynolds number values, the smallest value of TE (TE = 3) lies closest to the experimental data. However, for higher Mach numbers (Figs. 11-12), the opposite is true.
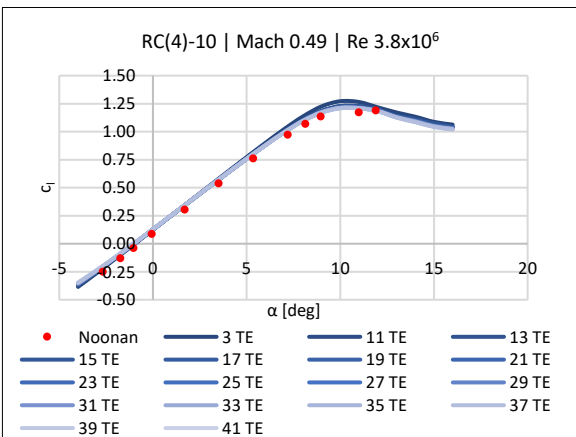
Figure 11. Lift coefficient versus angle of attack for the RC(4)-10 airfoil at $M = 0.49$ and $Re = 3.8 \times 10^6$.
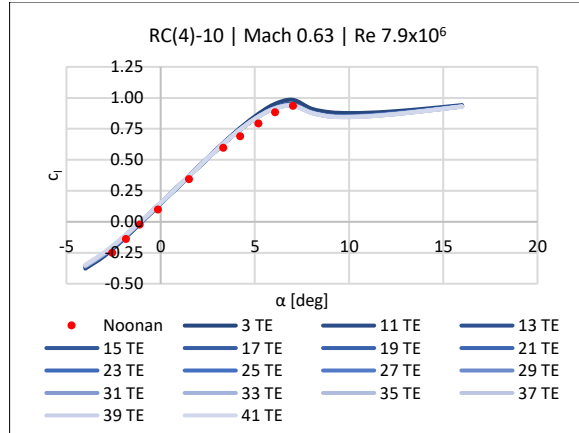
Figure 12. Lift coefficient versus angle of attack for the RC(4)-10 airfoil at $M = 0.63$ and $Re = 7.9 \times 10^6$.

As the trailing edge grid density is increased, the curve approaches the experimental test data, correlating quite well in comparison. In Figure 12, increasing the value of TE converges to the same lift coefficient trend. Increasing the number of trailing edge points ultimately results in a lift curve that more closely aligns with experimental data. For this reason, a trailing edge clustering of 33 was selected for all three airfoils (beyond this, the results appear to be very similar). With respect to both the 0012 and RC(4)-10, additional considerations are required to improve OVERFLOW results with experimental test data, the primary consideration being the manner with which AFTGen generates a grid for OVERFLOW. The grid generator may affect the overall quality of the grid used for the flow solver. Figure 13 depicts the overall grid for the RC(4)-10 airfoil for 11 trailing edge points and 33 trailing edge points.
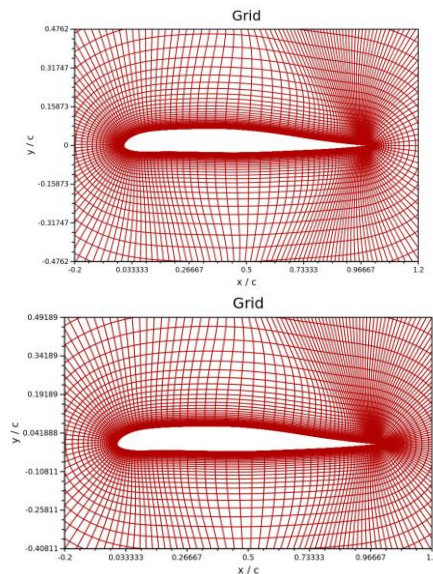
Figure 13. Effect on the overall RC(4)-10 grid for 11 TE points (top) and 33 TE points (bottom).

AFTGen's default clustering iterations value is 10,000. The number of iterations was increased in increments of 5,000 up to 60,000. Figure 14 and Figure 15 show the change in lift vs alpha plot with increasing clustering iterations for the NACA 0012 airfoil.
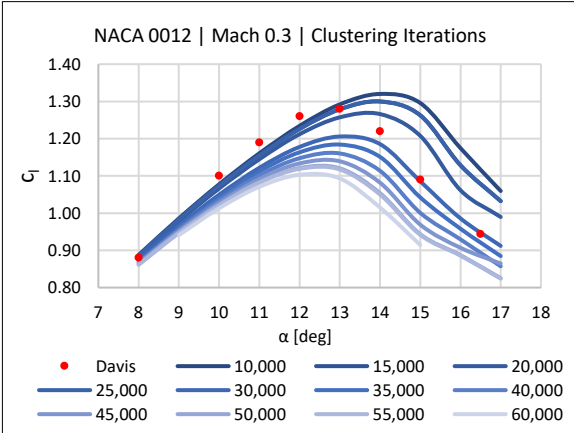

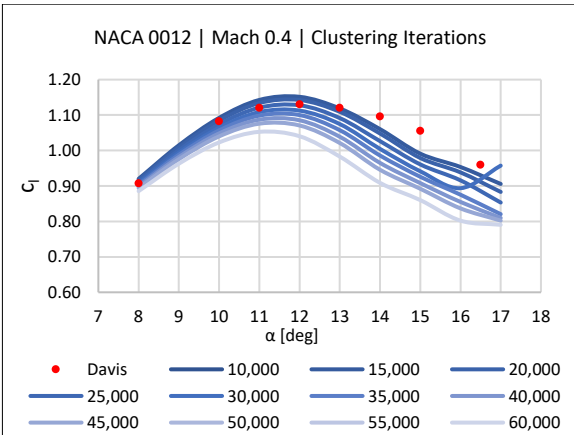**Figure 14. Change in CI for the NACA 0012 at M = 0.3 and Re/M = 5.2x10^6.**

Figure 15. Change in CI for the NACA 0012 at M = 0.4 and Re/M = 5.2x10^6.

While the clustering iterations seem to have no impact on accuracy when comparing simulations and experimental test data. In fact, increasing the CI results in a worse correlation per 5,000 iterations. Increasing clustering iterations reduces the predicted maximum lift coefficient significantly, with no change in the end result's correlation with legacy 0012 airfoil table data. An investigation of the clustering iterations was performed for the RC(4)-10 and SSC-A09. Figure 16 and Figure 17 show the results of increasing clustering iterations at Mach 0.44 for the RC(4)-10 airfoil.
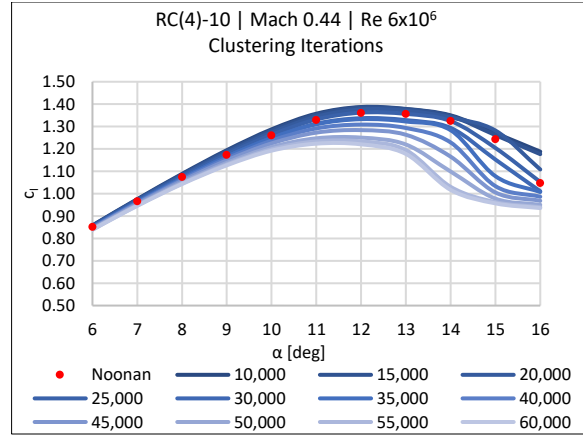
Figure 16. RC(4)-10 clustering iterations study at M = 0.44 and Re = 6x10^6, c_l vs α.

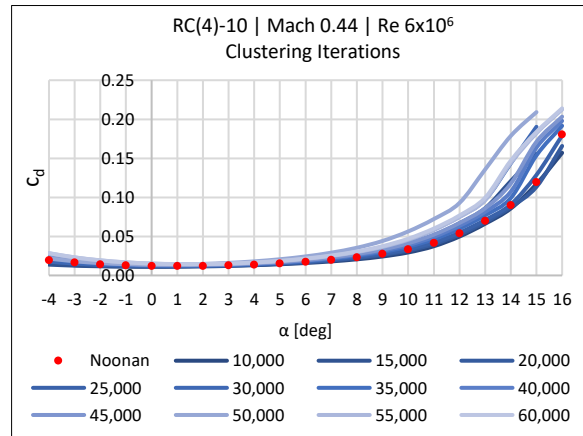**Figure 17. RC(4)-10 clustering iterations study at M = 0.44 and Re = 6x10^6, c_d vs α.**

For the RC(4)-10 airfoil, a trend similar to the 0012 is seen, with the exception that at 20K CI, there is a fairly good approximation of both the section lift and section drag coefficients. As the clustering iterations increase, the accuracy with between the OVERFLOW results and the experimental data decreases. With increasing clustering iterations, the lift is consistently underpredicted and drag is consistently overpredicted after 20,000 clustering iterations. Figure 18 provides a close up of the leading edge of the RC(4)-10 airfoil with increasing clustering iterations.
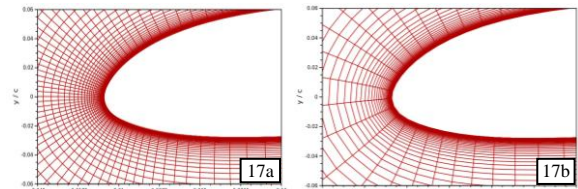

Figure 18. CI at the leading edge; 17a: 20K CI; 17b: 60K CI.

Up to 20K CI, there is a slight improvement to the grid at the leading edge. Beyond this, the grid seems to grow coarser as the number of clustering iterations increase. For both the NACA 0012 and the RC(4)-10 airfoils, the increase in clustering iterations results in a degradation of the lift curve slope. This trend also is seen when performing the same study with the SSC-A09 airfoil. Figure 19 and Figure 20 show the lift and drag coefficient versus angle of attack, with the experimental data not aligning as well with OVERFLOW simulations.
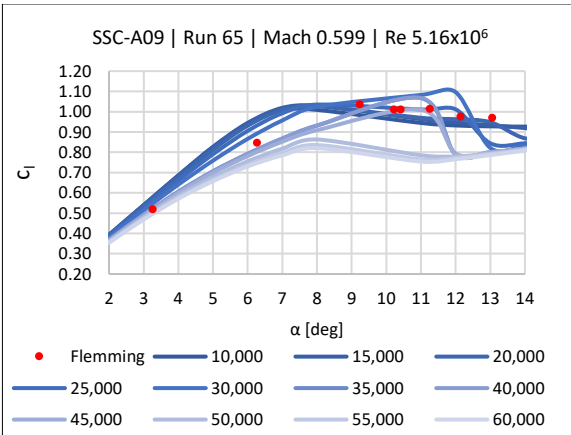
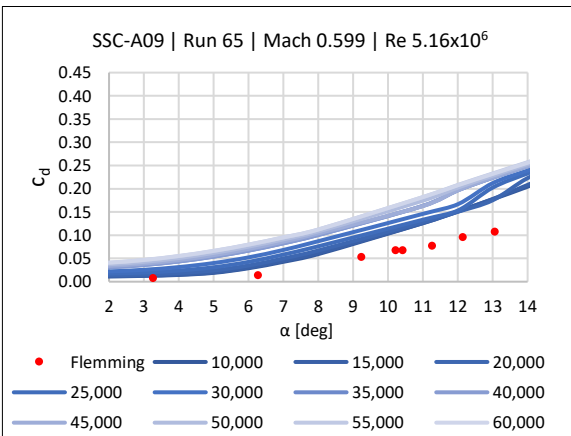**Figure 19. SSC-A09 clustering iterations study, Run 65 at $M = 0.599$ and $Re = 5.16x10^6$, c_l vs α.**

Figure 20. SSC-A09 clustering iterations study, Run 65 at $M = 0.599$ and $Re = 5.16x10^6$, c_d vs α.

The first few clustering iterations, from 5,000 to around 25,000, yield similar results with dramatic changes in the lift curve and the drag bucket with increasing iterations. The correlation is the worst for the SSC-A09 experimental and simulated data, and for this airfoil, the effect of increasing clustering iterations is inconclusive until further investigation can be performed.

RESULTS AND DISCUSSION

The following sections presents results generated using AFTGen with the XFOIL and OVERFLOW flow solvers. The NACA 0012, RC(4)-10, and SSC-A09 experimental data is compared against section lift and section drag coefficients calculated by XFOIL and OVERFLOW for a range of alpha-Mach pairs, discussed in more detail later. In addition, a comparison of the pressure coefficient for each airfoil is provided for validation of the computational approach used in this study.

The experimental pressure coefficient data in the NACA 0012 study originates from transition-free data as presented by Harris [Ref. 4]. Section lift and drag coefficients originate from the Davis [Ref. 5] produced airfoil table. The experimental section lift coefficient, section drag coefficient, and pressure coefficient distribution for the RC(4)-10 was digitized manually from data published by Noonan [Ref. 6]. The SSC-A09 experimental data, as detailed by Flemming [Ref. 7] was digitized from tabulated data on the pressure derived lift coefficient and wake rake derived drag coefficient, with the pressure data digitized manually from available pressure coefficient versus chord plots.

NACA 0012

The NACA 0012 cases were run at a Reynolds-Mach proportionality constant of $5.2x10^6$, which indicates that the Reynolds number is scaled with the Mach number. Cases were run fully turbulent and using the Coder transition model in OVERFLOW. Based on the previous studies, 33 TE points and 20,000 CI were used for all of the NACA 0012 OVERFLOW cases, and 400 panels were used for the XFOIL results.

Cases were run at Mach numbers from 0.2 to 1.0 at 0.1 intervals, with additional individual Mach numbers of 0, 0.18, 0.28, 0.38, 0.48, 0.62, 0.72, 0.75, 0.77, 0.82, and 0.92 selected to match established table data for all aerodynamic coefficients. The angle of attack range was -20 deg to 20 deg, for a total of 2,583 α-Mach pairs. Lift coefficient versus angle of attack plots for Mach 0.3, 0.5, and 0.75 and drag coefficient versus angle of attack plots for 0.28, 0.48, and 0.72 are presented as data representative of the complete table. Figure 21 shows the lift coefficient versus angle of attack curve for Mach 0.3.
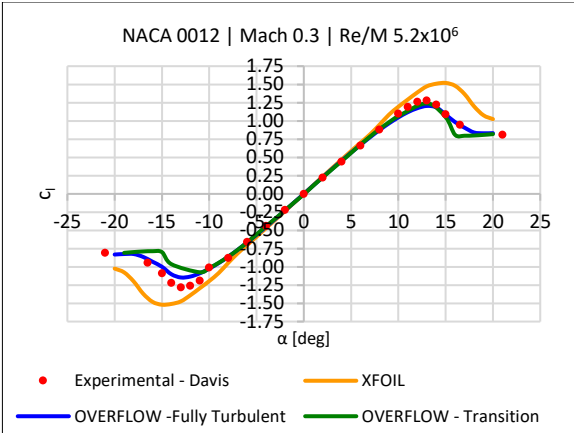
Figure 21. NACA 0012 lift curve at M = 0.3.

At M = 0.3, the maximum lift coefficient determined by XFOIL is overpredicted when compared with the baseline NACA 0012 data and the OVERFLOW calculations and occurs at a higher angle of attack. At this Mach number OVERFLOW correlates very well with experimental data in the positive angle of attack range using both the fully turbulent and transition models. In general, OVERFLOW's fully turbulent model does a better job predicting the lift coefficient in the stall region than the transition model does at this Mach number. Figure 22 displays the lift curve at Mach 0.5.
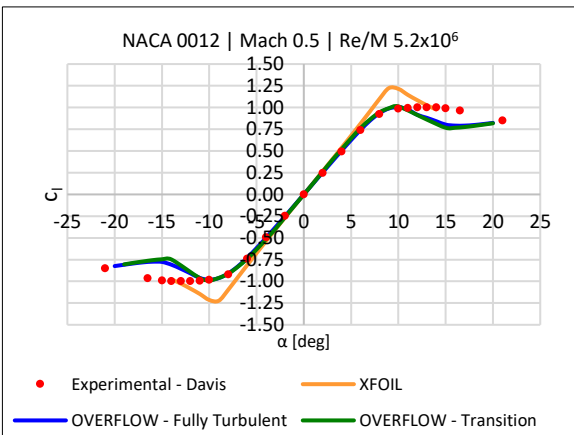
Figure 22. NACA 0012 lift curve at M = 0.5.

At M = 0.5 and particularly at higher angles of attack, XFOIL's capability reduces to a more limited angle of attack range from -14 deg to 14 deg, and after about 7 deg angle of attack, begins to overpredict lift when compared to experimental data and the OVERFLOW numerical models. The OVERFLOW fully turbulent and transition results show close predictions for $c_{l,max}$ at Mach 0.5, but there is a clear difference in trend in this stall region, where the NACA 0012 experimental data flattens out. XFOIL and both OVERFLOW models agree well from around -5 deg to 5 deg angle of attack. The OVERFLOW

and transition results correlate well from -10 deg to 10 deg angle of attack. Beyond this, the airfoil stalls, with OVERFLOW predicting the maximum lift coefficient close to baseline data, but at a lower stall angle of attack. Transition and fully turbulent results are also nearly identical. Beyond Mach 0.6, XFOIL was only able to converge for an increasingly limited range of angles of attack, and for this reason, Mach number comparisons beyond 0.6 do not include XFOIL results. Figure 23 display the lift curve at Mach 0.75.
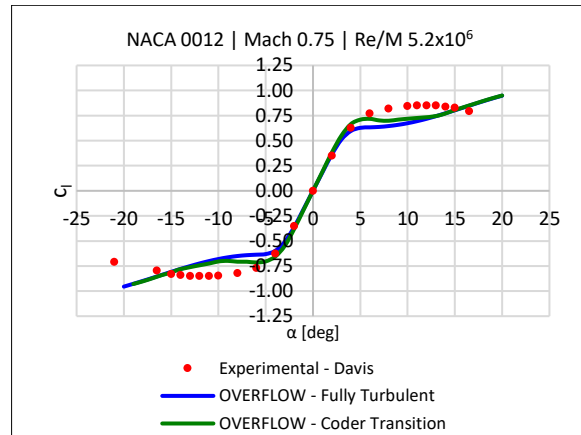

Figure 23. NACA 0012 lift curve at M = 0.75.

In Figure 23, a distinct difference in predicted c_{lmax} is seen, similar to the case at Mach 0.5. Predictions for both OVERFLOW models are almost identical, with the exception of the stall region. At M = 0.75, the trend in the experimental data does not depict a conventional stall curve – instead, the NACA 0012 experimental data set shows a much more gradual change in lift for angles of attack beyond 4 deg; although not shown here, as the Mach number increases, the lift curve peaks at decreasingly small angle of attack values. There appears to be a slight offset between the fully turbulent predictions and the transition model, with the transition model predicting a lift coefficient slightly greater than the fully turbulent model after about 3 deg angle of attack. Overall, for the NACA 0012 airfoil, XFOIL compares reasonably well with the experimental test data within the linear angle of attack range. This is expected, based on its limitations in the stall region. OVERFLOW shows good correlation with experimental data in this linear alpha range as well as $c_{l,max}$ up until Mach 0.5. At Mach 0.5 and beyond, the stall region from the experimental data shows a much more gradual decrease in lift than was expected, and for this reason, the overall trends do not align well beyond the linear angle of attack range. This is an area of uncertainty that still needs to be investigated.

The drag coefficient was calculated in XFOIL and OVERFLOW for Mach numbers at 0.18, 0.28, 0.38, 0.48, 0.62, 0.72, 0.77, and 0.82. XFOIL was able to converge

9

up to Mach 0.62. Figure 24, Figure 25, and Figure 26 show the drag coefficient versus angle of attack curves for Mach 0.28, 0.48, and 0.72.
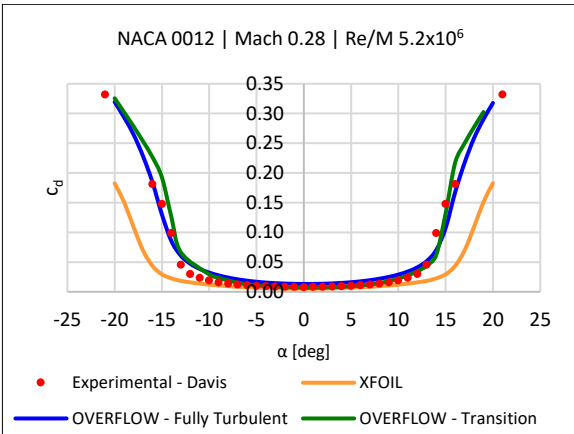

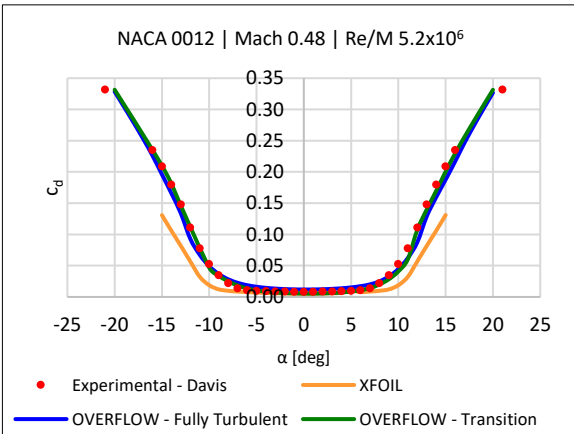**Figure 24. NACA 0012 section drag coefficient versus α curve at $M = 0.28$.**

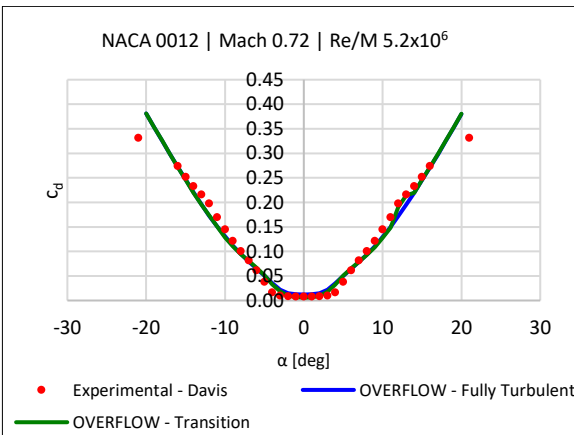**Figure 25. NACA 0012 section drag coefficient versus α curve at $M = 0.48$.**


Figure 26. NACA 0012 section drag coefficient versus α curve at $M = 0.72$.

In all cases, XFOIL tended to underpredict drag in the drag bucket. OVERFLOW, on the other hand, shows that the transition model tends to yield section drag coefficients closer to the experimental data than the fully turbulent model at lower angles of attack, with a slight offset as the angle of attack exceeds ±10 deg. OVERFLOW comes closest to the experimental results at Mach numbers from 0.28 through 0.72, with data and trends aligning well. At Mach 0.72 there is a difference in overall trend between simulated and experimental test results at higher angles of attack.

As a sanity check for the approach, an investigation into the pressure coefficient was completed. Unfortunately, the Davis NACA 0012 .c81 table referenced in this report does not have a set of pressure data for comparison. For this reason, pressure data from Harris et al. [Ref. 3] was used to validate the simulation results. The Davis data was used for comparison of AFTGen with OVERFLOW .c81 table results because it contained the greatest range of alpha-Mach pairs. The Harris data contains a limited range of transition-free data, with the rest of the data representing fixed-transition testing. Since only fully turbulent and Coder transition models were of interest, the transition-free Harris data was used for comparison with fully turbulent OVERFLOW results.

Cases were run to match the Harris testing conditions at a Reynolds number of $3x10^6$ and at an angle of attack of -0.14 deg (as close to 0 deg as available with experimental data). The Mach numbers selected were Mach 0.3 and 0.6 so that comparisons between incompressible and compressible flow could be made. The airfoil is symmetric, so distinguishing between the upper and lower surface pressures of the airfoil was difficult, as the data was digitized from the plots in the report. The primary goal with looking at the pressure coefficient was a validation of the approach used for OVERFLOW calculations.

Figure 27 and Figure 28 show the pressure coefficient versus chord, with the experimental data shown by the red symbols, XFOIL shown in yellow, and OVERFLOW's fully turbulent results depicted by the blue curve.
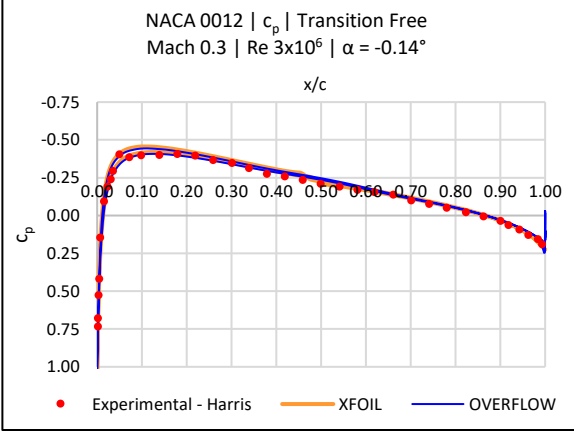
Figure 27. C_P vs x/c for the NACA 0012 airfoil at M = 0.3. Experimental data digitized from Figure 40a [Ref. 4]
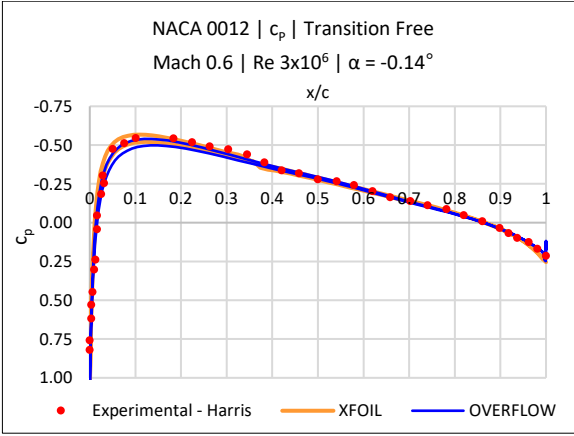
Figure 28. C_P vs x/c for the NACA 0012 airfoil at M = 0.6. Experimental data digitized from Figure 40e [Ref. 4].

The Reynolds-Mach pair at Mach 0.3 shows excellent agreement between the test data, XFOIL, and OVERFLOW results. At Mach 0.6, the agreement is fairly good between XFOIL and the experimental data, although XFOIL slightly overpredicts the peak pressure coefficient. OVERFLOW captures the pressure coefficient well, although there is also a sharp spike in c_P at the trailing edge, which ultimately needs to be explored; the most likely cause could be the periodic boundary condition at the trailing edge. After comparing these plots, the flow was visualized to generate the velocity and pressure contours. Figure 29 depicts c_P contours for OVERFLOW's fully turbulent model at Mach 0.3, with the pressure set as the scalar and the velocity as the vector.
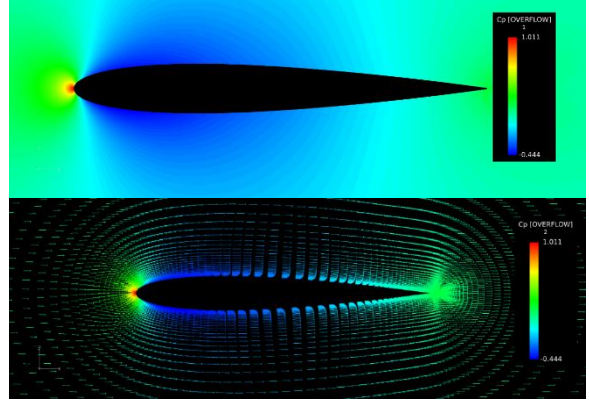
Figure 29. Pressure coefficient contour and vector plots at M = 0.3 for the NACA 0012.

The stagnation point at the leading edge of the airfoil shows the OVERFLOW calculated pressure coefficient value of 1.011. In Figure 29, the Harris data showed a peak c_P around 0.7, which is overall lower than is shown in the OVERFLOW results. The pressure coefficient can be calculated directly using relationships between stagnation pressure, Mach number, and specific heat ratio, depicted in equation 1 as used for incompressible flow [Ref. 12]:

$$C_P = \frac{P - P_\infty}{\frac{1}{2}\rho_\infty v_\infty^2} \tag{1}$$

Equation 1 can be further simplified into equation 2:

$$C_P = \frac{P - P_\infty}{\frac{1}{2}\rho_\infty v_\infty^2} \rightarrow \frac{P_\infty(\frac{P_0}{P_\infty}-1)}{\frac{1}{2}\gamma P_\infty M_\infty^2} \rightarrow \frac{2(\frac{P_0}{P_\infty}-1)}{\gamma M_\infty^2} \rightarrow C_P = \frac{2}{\gamma M_\infty^2}\left(\frac{P_0}{P_\infty} - 1\right) \tag{2}$$

where p_0 is the total pressure and p_∞ is the static freestream pressure. Using equation 2, the calculated stagnation pressure coefficient is 1.023. This shows that at this Mach number, OVERFLOW slightly underpredicts the pressure coefficient at the stagnation point. Figure 30 shows the c_P contours at Mach 0.6 for OVERFLOW's fully turbulent model, with the pressure set as the scalar and the velocity as the vector. The contours show the pressure distribution and pressure gradient across the airfoil surface.
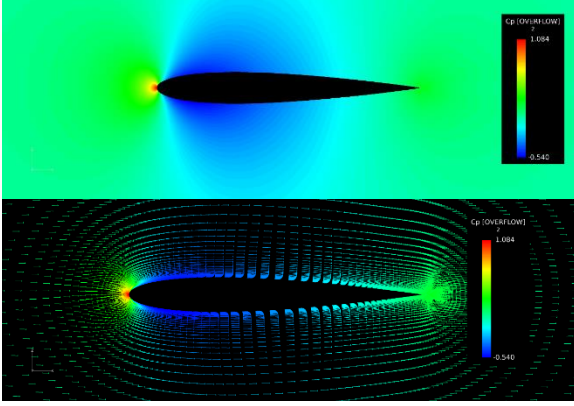
Figure 30. Pressure coefficient contour and vector plots at M = 0.6 for the NACA 0012.

No adverse pressure gradient is shown, indicating at this Mach number and angle of attack, no flow separation occurs. Using equation 2, the pressure coefficient can be calculated and compared with experimental and simulated results. The Harris data provides a pressure coefficient of 0.88 at the leading edge, OVERFLOW calculates the stagnation pressure coefficient as 1.084. For comparison, the pressure coefficient is again calculated using the formula for pressure coefficient at the stagnation point, however with equation 3, which is valid for compressible flow [Ref. 12]:

$$C_P = \frac{2}{\gamma M_\infty^2}\left[\left(1 + \frac{\gamma-1}{2}M_\infty^2\right)^{\frac{\gamma}{\gamma-1}} - 1\right] \tag{3}$$

Using formula 3, the pressure coefficient at Mach 0.6 was determined to be 1.093. OVERFLOW again underpredicts the pressure. The full list of calculated stagnation pressure coefficients is included in Table 3.

Table 3. Calculated stagnation pressure coefficients at all Mach numbers for the NACA 0012 airfoil.

| M	$C_{P,\text{stag}}$
0.10	1.0025
0.18	1.0081
0.20	1.0100
0.28	1.0197
0.30	1.0227
0.38	1.0366
0.40	1.0406
0.48	1.0588
0.50	1.0639
0.60	1.0929
0.62	1.0994
0.70	1.1278
0.72	1.1356
0.75	1.1476
0.77	1.1560
0.80	1.1691
0.82	1.1781
0.90	1.2171
0.92	1.2275
1.0	1.2722

RC(4)-10

The RC(4)-10 airfoil simulations were run for fewer α-Mach pairs, with the details on angle of attack, Mach number, and Reynolds number included in Table 4.

Table 4. RC(4)-10 primary inputs for XFOIL and OVERFLOW.

| Simulation #	α range (Δ1°)	Mach	Re
1	-4° to 16°	0.34	3.9×10^6
2	-4° to 16°	0.34	4.8×10^6
3	-4° to 16°	0.37	3.8×10^6
4	-4° to 16°	0.39	3.8×10^6
5	-4° to 16°	0.39	5.4×10^6
6	-4° to 16°	0.42	3.8×10^6
7	-4° to 16°	0.42	5.7×10^6
8	-4° to 16°	0.44	3.8×10^6
9	-4° to 16°	0.44	6.0×10^6
10	-4° to 16°	0.49	3.8×10^6
11	-4° to 16°	0.49	6.6×10^6
12	-4° to 16°	0.59	7.0×10^6
13	-4° to 16°	0.63	7.9×10^6
14	-4° to 16°	0.69	8.3×10^6
15	-4° to 16°	0.73	8.5×10^6
16	-4° to 16°	0.78	8.8×10^6

The simulations will be referred to by the simulation number provided in Table 4. Simulations 1, 3, 4, 6, 8, 10, and 12-16 were run at a constant stagnation pressure of 60 psia, while Simulations 2, 5, 7, 9, and 11 were based on experimental data at stagnation pressures ranging from 48 to 36 psia. In the interest of brevity, only three Mach-Reynolds pairs (Simulations 2, 9, and 12) will be focused on here. The lift coefficient versus angle of attack curve for simulation 2 is shown in Figure 31, with experimental data shown in red, XFOIL in orange, OVERFLOW fully turbulent in blue, and OVERFLOW transition in green.
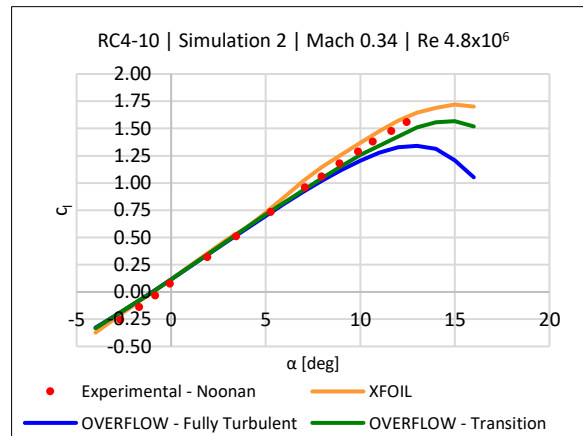
Figure 31. RC(4)-10 lift curve at Mach 0.34 and a Reynolds number of 4.8×10^6.

Figure 31 shows that for simulation 2, at Mach 0.34, there is fairly good agreement between OVERFLOW and the

experimental dataset until the angle of attack reaches around 10 deg. With XFOIL, the lift coefficient calculations correlate well, but there is an offset seen between the solver and the test data at negative angles of attack and at an angle of attack around 5 deg. This results in XFOIL moderately overshooting the lift coefficient. OVERFLOW's transition model correlates well with the test data, performing a bit better than the fully turbulent model at this Mach number. The fully turbulent method shows the greatest discrepancy in calculated section lift coefficient. At this Mach-Reynolds pair, the test data did not contain angles of attack beyond about 13 deg, so experimental testing did not capture stall conditions for comparison. One thing to consider is that the lift curve slope for all solvers has a slight offset from the negative angles of attack up until around 1 to 2 deg. This could be an artifact of the digitization process using the web plotter tool that estimated the data points from the Noonan report. This offset is not seen as dramatically in Figure 32, where simulation 9 shows the lift curve at Mach 0.44.
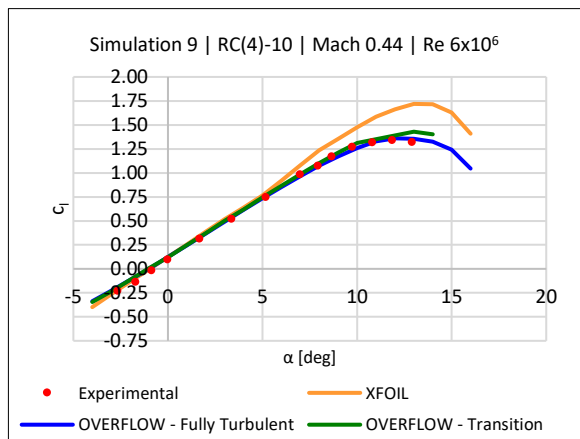
Figure 32. RC(4)-10 lift curve at Mach 0.44 and a Reynolds number of 6x10^6.

At Simulation 9's Mach-Reynolds pair , the discrepancy between XFOIL calculations compared to OVERFLOW and experimental data increases. Beyond an angle of attack around 6 deg, XFOIL overpredicts lift. OVERFLOW's transition and fully turbulent models align very closely with one another as well as the experimental test data, with a slight overprediction in lift for the entire angle of attack range. The overall trend for the fully turbulent method matches that of the experimental data set, and the likely cause for the offset is with the manual digitization process. Figure 33 depicts the lift versus angle of attack curve for simulation 12 at Mach 0.59.
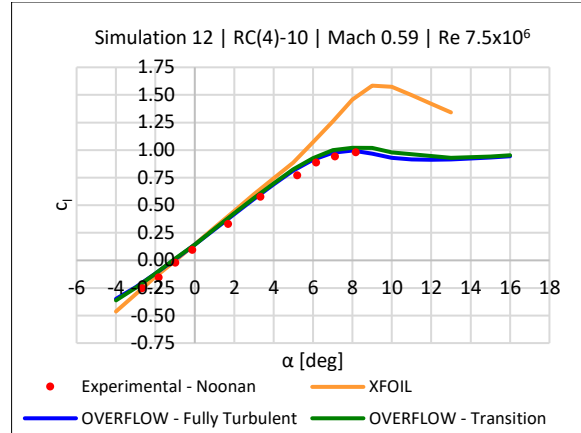
Figure 33. RC(4)-10 lift curve at Mach 0.59 and a Reynolds number of 7.5x10^6.

At the Mach-Reynolds pair depicted in Simulation 12, XFOIL significantly overpredicts the section lift coefficient beyond an angle of attack around 4 deg. OVERFLOW's transition and fully turbulent models align very closely with one another as well as the experimental test data, with a slight overprediction in lift from around 9 deg angle of attack onward. The overall trend for the fully turbulent method matches that of the experimental data set.

The next set of figures show the drag polar for the airfoil, with the digitized Noonan data depicted by the red symbols, XFOIL in orange, OVERFLOW fully turbulent in blue, and OVERFLOW transition in green. Figure 34, Figure 35, and Figure 36 compare the Noonan digitized data with XFOIL results (within its Mach number limits) and OVERFLOW results (both fully turbulent and transition models).
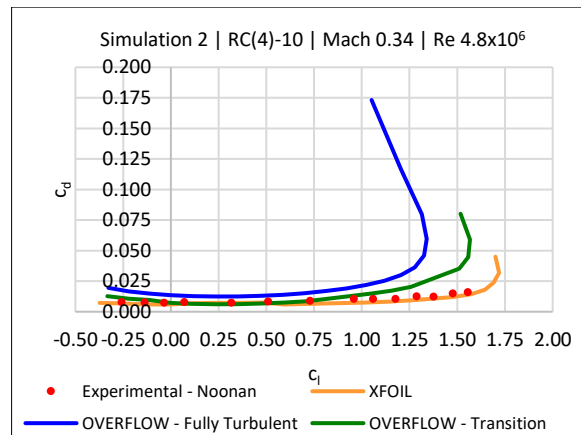
Figure 34. RC(4)-10 drag bucket at Mach 0.34 and a Reynolds number of 4.8x10^6.
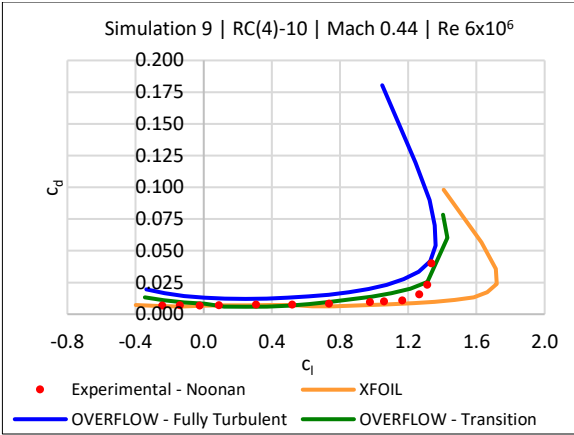
Figure 35. RC(4)-10 drag bucket at $M = 0.44$ and a Reynolds number of 6×10^6.
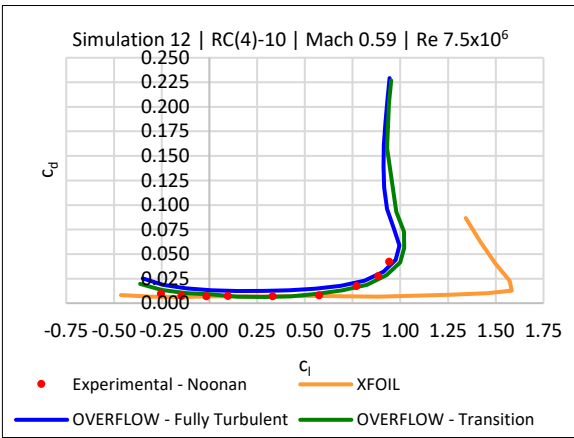

Figure 36. RC(4)-10 drag bucket at Mach 0.59 and a Reynolds number of 7.5×10^6.

XFOIL correlates best with the test data at Mach numbers below 0.4. At Mach 0.34, the experimental data shows the same trend and lies fairly close to the XFOIL curve, with XFOIL slightly underpredicting the drag overall. At higher angles of attack and as Mach number increases beyond Mach 0.34, XFOIL (as mentioned earlier in this section) tends to underpredict drag. This trend is shown in all drag polars, with the largest discrepancies seen as the Mach number approaches transonic conditions. This is not surprising, as XFOIL is not designed to analyze flow at transonic speeds and is known to not be as reliable at large angles of attack. At Mach numbers from 0.34 through 0.44, fully turbulent simulations overpredict drag, while the transition model results match up quite well in the linear angle of attack range, with some discrepancy in drag seen as the curve approaches maximum lift. At Mach numbers at 0.59 and above, the fully turbulent and transition results show nearly identical trends. For these Mach numbers, the fully turbulent results are consistent in overpredicting drag slightly. At this particular Mach number, there is excellent correlation between the experimental curve and

both OVERFLOW model types, with the transition model's drag polar aligning closest to Noonan's test data.

In addition to the lift curve and drag polar, a study of the pressure coefficient was completed for the RC(4)-10 for the same Mach-Reynolds pairs. First, the stagnation pressure coefficient was calculated using equation 3, applicable for compressible flow as described in the previous section. The angles of attack selected are the values as close to zero deg as possible at -0.13, -0.10, and -0.08 deg. Figures 37 shows the pressure coefficient versus chord for the RC(4)-10 at Mach 0.34.
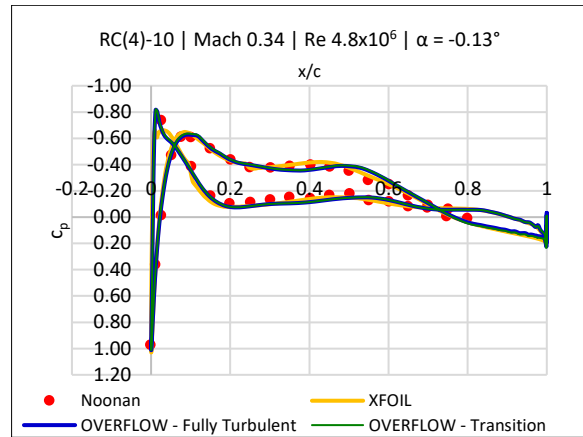

Figure 37. C_P vs x/c for the RC(4)-10 airfoil at Mach 0.34 and Re 4.8×10^6.

At $M = 0.34$, XFOIL slightly overpredicts peak pressure coefficient and overpredicts the maximum pressure coefficient at the leading edge, with fairly good agreement for the upper and lower surfaces of the airfoil. The transition and fully turbulent models yield nearly identical results that align well experimental test data, with a slightly underpredicted pressure coefficient at the leading edge. Figure 38 and Figure 39 show the pressure coefficient versus chord for Mach 0.44 and Mach 0.59.
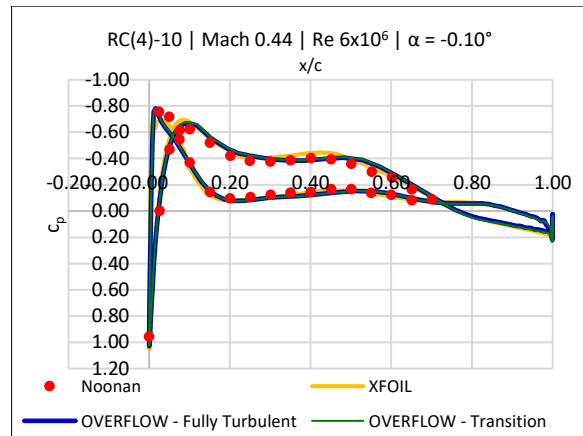

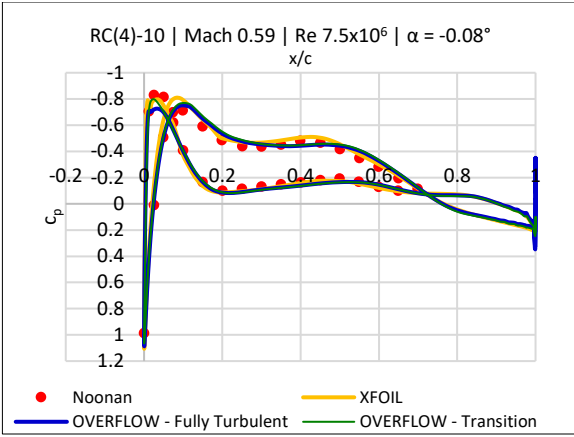**Figure 38. C_P vs x/c for the RC(4)-10 airfoil at Mach 0.44 and Re 6×10^6.**

Figure 39. C_P vs x/c for the RC(4)-10 airfoil at Mach 0.59 and Re $7.5x10^6$.

At Mach 0.44, both OVERFLOW models show acceptable agreement with the pressure coefficient data, with the exception of the slight overprediction of the maximum pressure coefficient at the leading edge. XFOIL pressure coefficient calculations compare well with measurements across the chord of the airfoil, with the largest differences seen at the pressure coefficient peak (where XFOIL slightly underpredicts the value) and right around 40% chord, were the pressure is slightly overestimated. At Mach 0.59, a similar trend is shown for XFOIL, with the difference seen at the leading edge, where the pressure coefficient at the first peak is much closer to the experimental value. There is still a slight overprediction of the pressure around 40% chord, but the overall trend agrees well with both OVERFLOW solvers and the experimental data. Unlike the Mach 0.44 case, OVERFLOW's transition model is able to capture the first peak pressure coefficient better than the fully turbulent model, but otherwise yields pressure calculations very close to the fully turbulent model and experimental data set. These differences, as mentioned previously, could simply be a result of some margin of error in the digitization of the experimental data set.

These plots were created to show the pressure coefficient at an angle of attack as close as possible to 0 deg to compare with the hand calculated stagnation pressure coefficient. As a refresher, equation 3 was used to calculate the stagnation pressure coefficient. Table 5 lists the stagnation pressure coefficient calculated for the RC(4)-10 at all tested/simulated Mach numbers.

Table 5. Calculated stagnation pressure coefficients at all Mach numbers for the RC(4)-10 airfoil.

M	$C_{P, stag}$
0.34	1.0292
0.37	1.0346
0.39	1.0385
0.42	1.0448
0.49	1.0613

Table 5 continued	
0.54	1.0748
0.59	1.0897
0.63	1.1027
0.69	1.1240
0.73	1.1395
0.78	1.1603
0.83	1.1828

The calculated value provides a way to check the OVERFLOW, XFOIL, and experimental data results for the stagnation pressure coefficient. In all the pressure coefficient plots, there is relatively good agreement between the experimental data and the XFOIL and OVERFLOW results. Note that the experimental data pressure coefficient is an estimate, given that the plots in the report were often not clear in the region near the leading edge, resulting in subjectivity when digitizing the plots.

SSC-A09

Multiple runs were set up from tabulated data available in the NASA/TM by Flemming [Ref. 7]. The run number, total pressure p_0, angle of attack, Mach number, and Reynolds number used in simulations and hand calculations are shown in Table 6.

Table 6. SSC-A09 inputs for XFOIL and OVERFLOW.

Run #	α range (Δ1°)	Mach #	Re
60	-1° to 7°	0.399	$3.85x10^6$
61	0° to 16°	0.307	$4.29x10^6$
63	-6° to 20°	0.500	$4.57x10^6$
65	-5° to 14°	0.599	$5.16x10^6$
68	-1° to 16°	0.603	$5.21x10^6$
69	-4° to 12°	0.703	$5.73x10^6$
70	-4° to 9°	0.804	$6.11x10^6$

The experimental data were plotted using the available tabulated data in the report, with two sets of aerodynamic coefficients provided for use. Flemming provides pressure derived lift, drag, and moment coefficients, as well as the balance derived lift, drag, and moment coefficients. The only coefficients of interest, and as such, discussed in this report, are the pressure derived aerodynamic coefficients. Similarly, only configuration 2 cases are considered, with configuration 2 described as the clean airfoil configuration in the wind tunnel test. The analysis for this airfoil will primarily discuss the lift curves and drag polars.

In all figures, red represents experimental data from the Flemming report, orange represents XFOIL, blue indicates OVERFLOW's fully turbulent model, and green indicates OVERFLOW's Coder transition model. Run 60 in this experiment covered a limited angle of attack run and only includes the linear angle of attack

range, with only a few data points available for comparison. Figure 40 and 41 show the lift coefficient versus angle of attack and drag coefficient versus angle of attack for Run 60.
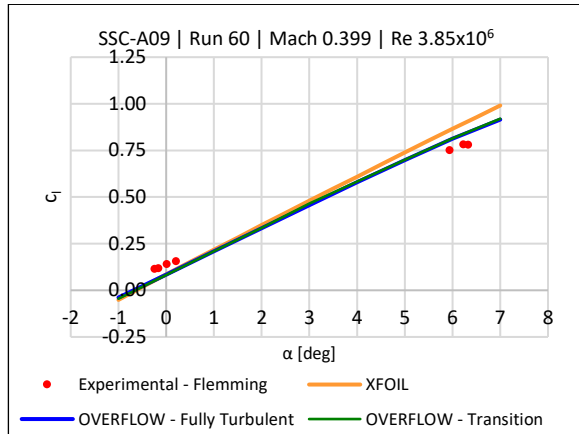

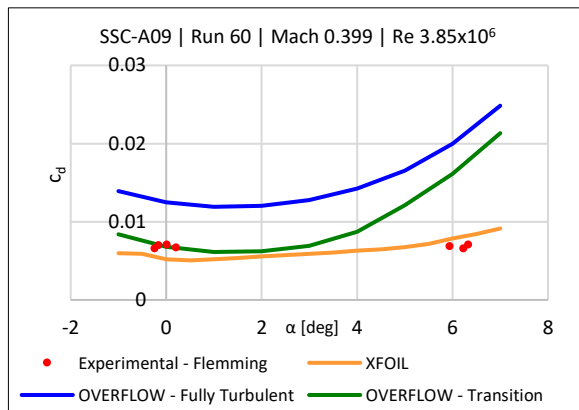**Figure 40. SSC-A09, c_l versus α, Run 60, Mach 0.399, Re 3.85x10^6.**

Figure 41. SSC-A09, c_d versus α, Run 60, Mach 0.399, Re 3.85x10^6.

Normally, this would suggest that there would be good agreement between the simulations and experimental test data, but for this airfoil, this is not the case. In Run 60, XFOIL underpredicts lift below an angle of attack of 1.5 deg, but overestimates the lift beyond 2.5 deg, leaving a limited region where there is some overlap between XFOIL calculations and experimental test data. With respect to the OVERFLOW results, the fully turbulent and transition models overlap XFOIL results from -1 to 1.5 deg but underestimates the lift coefficient in this range. Beyond an angle of attack of 2.5 deg, the OVERFLOW models predict very similar lift coefficients, but overpredict the values recorded in the wind tunnel test. The overprediction is seen much more clearly on the drag polar in Figure 41. The drag polar shows that the fully turbulent model significantly overpredicts drag, while the XFOIL and transition model show drag and lift calculations more in the ballpark of the

experimental data, although with not much commonality in curve trends. Figure 42 and Figure 43 show the test data lift and drag curves plotted with XFOIL and OVERFLOW data for Run 63, at Mach 0.5 and a Reynolds number of 4.57x10^6.

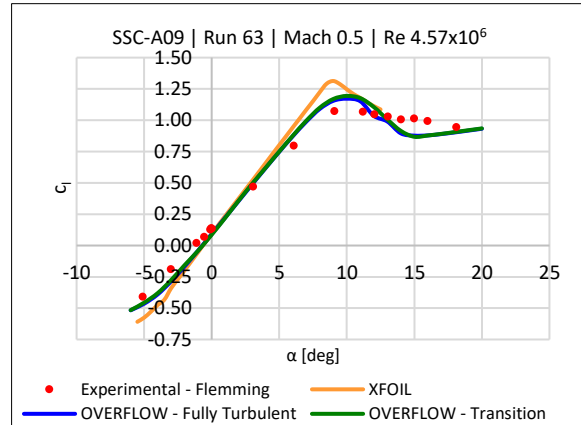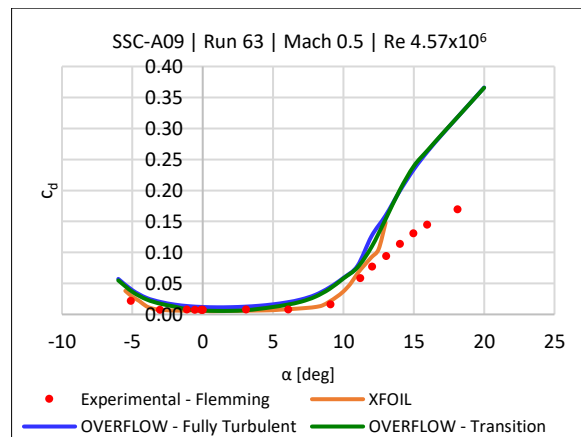**Figure 42. SSC-A09, c_l versus α, Run 63, Mach 0.5, Re 4.57x10^6.**

Figure 43. SSC-A09, c_d versus α, Run 63, Mach 0.5, Re 4.57x10^6.

For this run, the lift curve shows that both XFOIL and OVERFLOW underpredict lift below an angle of attack around 1 deg, with XFOIL showing a greater discrepancy in lift compared with the OVERFLOW cases. Beyond this same angle of attack, the opposite is true – the lift curve is overpredicted, with XFOIL showing a greater discrepancy in lift than the fully turbulent and transition models. OVERFLOW calculates the maximum lift coefficient around the same angle of attack range, while XFOIL significantly overpredicts a higher maximum lift coefficient at an earlier stall angle of attack. The maximum lift coefficient predicted by the experimental data, XFOIL, OVERFLOW's fully turbulent model, and OVERFLOW's transition model are 1.121, 1.313, 1.172, and 1.190, respectively. With respect to the drag curve, XFOIL aligns fairly well with experimental data from -4

to 4 deg angle of attack. The XFOIL and experimental curve share a similar trend as well. The OVERFLOW fully turbulent and transition models are close in value and nearly identical in trend until the angle of attack approaches stall conditions. For the most part, drag is overpredicted by both OVERFLOW models, while XFOIL slightly overpredicts in the linear region (from -2 to 5 deg) and slightly overpredicts drag from 5 to 18 deg.

The lift and drag curves for Runs 65 are shown in Figure 44 and Figure 45. XFOIL is not included in these runs due to the very limited number of converged solutions for the α-Mach pairs of interest.
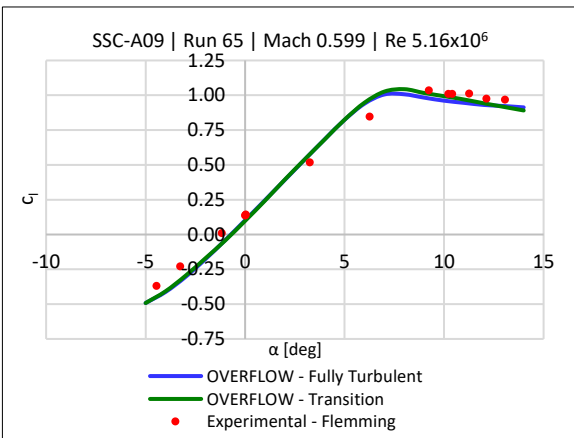
Figure 44. SSC-A09 lift coefficient versus angle of attack, Run 65, Mach 0.599, Re 5.16x10⁶.
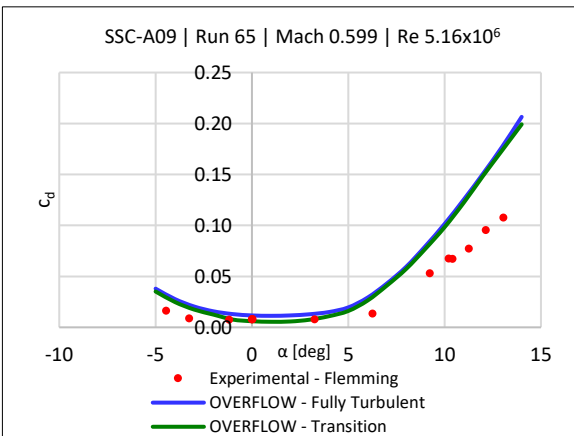
Figure 45. SSC-A09 drag coefficient versus angle of attack, Run 65, Mach 0.599, Re 5.16x10⁶.

For most of these runs, there is an overall weak comparison between the simulated data and the experimental test data, with a consistent trend of OVERFLOW underpredicting the lift for negative angles of attack, and overpredicting the lift at angles of attack beyond 1 deg. Run 65 shows the fully turbulent model overpredicting drag, with the transition model similarly overpredicting drag, with the exception of a small region

in the linear alpha range, where the minimum drag coefficient for the transition model is very close to what is derived in the experimental data set. This difference in drag calculations needs to be further investigated to determine the cause.

As performed for the other two airfoils, a stagnation pressure coefficient study was performed to compare the pressure coefficient calculations between the experimental dataset and the various flow solvers. Equations 2 and 3 were used to calculate the pressure coefficient, with the corresponding run numbers, Mach numbers, and stagnation pressure coefficients tabulated in Table 7.

Table 7. SSC-A09 hand calculated pressure coefficients.

Run #	Mach #	$c_{P, \text{stag}}$
60	0.399	1.0404
61	0.307	1.0238
63	0.500	1.0639
65	0.599	1.0926
68	0.603	1.0938
69	0.703	1.1290
70	0.804	1.1709

The data set did not include data at approximately zero angle of attack, so instead, plots from the Flemming report are digitized as available. XFOIL and OVERFLOW calculations were performed for the corresponding measured angle of attack. Figure 46 provides the experimental, XFOIL calculated, and OVERFLOW calculated pressure coefficients, while Figure 47 visualizes the pressure contours at a Mach number of 0.399.
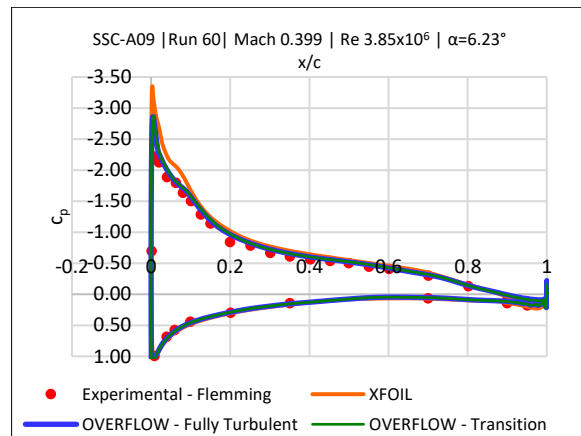
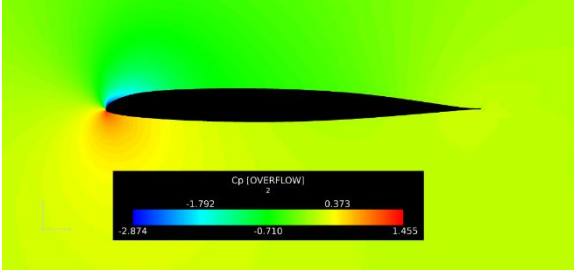**Figure 46. SSC-A09 pressure coefficient plot for Run 60.**

Figure 47. SSC-A09 pressure coefficient contour plot for Run 60.

Figure 49. SSC-A09 pressure coefficient contour for the Run 65.

For Run 60, the experimental stagnation pressure coefficient at the leading edge can be estimated at 1. XFOIL calculates the pressure coefficient at approximately 1.04. OVERFLOW overestimates this value at 1.455. Figure 46 shows that all solvers, overpredict the peak pressure coefficient, with XFOIL yielding a smaller estimate of this peak pressure coefficient. Fully turbulent and transition trends for OVERFLOW are nearly identical. OVERFLOW results correlate extremely well with the experimental pressure coefficient, matching the trend nearly identically aside from the stagnation pressure and trailing edge. XFOIL's pressure coefficient trend is not as accurate on the upper surface, with pressure overpredictions seen until about 15% chord. Figures 48 plots the experimental, XFOIL, and OVERFLOW pressure coefficients, while Figure 49 visualizes the pressure coefficient distribution across the airfoil for Run 65.
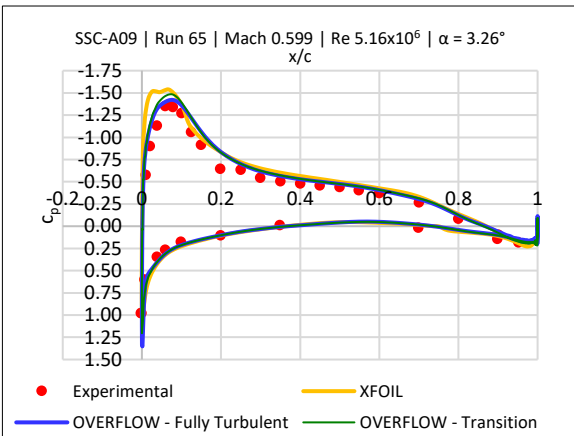
For Run 65, the experimental data set has an estimated leading edge stagnation pressure coefficient of 1, with XFOIL overpredicting the pressure coefficient at 1.1. OVERFLOW overpredicts the pressure coefficient as 1.35. In general, the trend for the OVERFLOW results is close to the experimental data set, with the pressure slightly underestimated on the upper airfoil. XFOIL shows a significant underestimate of the peak pressure, and a distinct different in trend until about 20% of the airfoil chord (from the leading edge). There is a tendency for both codes to overpredict the pressure coefficient on the upper surface of the airfoil.

CONCLUSIONS AND FUTURE WORK

One of the major takeaways from this study is the limitations of XFOIL. XFOIL is only valid for subsonic flows, so cannot accurately model transonic flow due to phenomenon like shocks that may occur. XFOIL is also limited in angle of attack range and cannot accurately model stall and post-stall conditions, because it is an inviscid flow solver and cannot calculate viscous drag. The results are consistent in nearly every case run with XFOIL, where the linear range is generally predicted well and the lift coefficient is overpredicted as the stall angle of attack approaches (with the exception being the generally poor correlation with most of the SSC-A09 cases). XFOIL, however, runs in seconds on a desktop computer. OVERFLOW is limited at low Mach numbers, and appears to perform best at Mach numbers of 0.4 and above. The exploration of airfoil table generation using XFOIL and OVERFLOW yielded moderately successful results for the NACA 0012 airfoil table, reasonably good results for the RC(4)-10 results, and questionable results for the SSC-A09. The SSC-A09 XFOIL and OVERFLOW results do not compare well with the experimental dataset, even considering the exploration of improvements to simulation approach with respect to clustering iterations, trailing edge points, and improvements in geometry. An individual grid study for the SSC-A09 airfoil was performed for future use of this research project, which will further contribute to a best practice guide for airfoil table generation.

Figure 48. SSC-A09 pressure coefficient plot for Run 65.

Another consideration is that this investigation focused on the capability of the XFOIL and OVERFLOW solvers using features built-in to AFTGen, with the takeaways from the study as follows:

- Ensure the leading-edge profile of the airfoil is sufficiently defined.
  a) If using AFTGen, consider that the grid generator may not refine the imported geometry adequately, so using additional points around the leading edge is helpful.
  b) Use a spline to add more points around the leading edge of the airfoil, up to 15%, on the upper and lower surfaces. This improved the overall correlation between experimental data and simulations for the RC(4)-10 airfoil.
- For OVERFLOW, ensure a blunt trailing edge contains enough points to define the grid in that region.
  a) A minimum of 11 trailing edge points should be used, per suggestions by Allan, Buning, and Romander (Oct. 2021)
  b) The trailing edge points are airfoil dependent – an independent study per airfoil is recommended.
- For OVERFLOW, Clustering iterations study is optional
  a) Increasing the clustering iterations showed no marked improvement in results for the 0012 and SSC-A09 airfoils, but 20,000 clustering iterations resulted in a small increase in accuracy for the RC(4)-10.
- Visualize the flow
  a) When possible, ensure that the pressure and Mach contours display reasonable results – contours should appear smooth and realistic for the conditions.
- Perform independent studies for each airfoil, as there is not a one-size-fits-all grid.

FUTURE WORK

A number of other features can be explored in the future to improve experimental and simulated data correlation. Considerations for future work include the following:

- Complete a study of Ncrit values in XFOIL.
- Import a grid for use in AFTGen and compare the AFTGen-generated grid and imported grid, focusing on grid point distribution around regions of high curvature.

- Complete a study of higher Reynolds number airfoils, such as the SC1095 and SC1094R8 using similar and/or improved methodologies.
- Explore the maximum stretching ratio of grid points and its effect on AFTGen's grid generator.
- Research low Mach preconditioning and improve OVERFLOW results at lower Mach numbers.

Although a best practice guide for airfoil table generation has not yet been developed, this present work is one of many projects that will be used toward that goal. A series of studies will need to be completed to improve OVERFLOW results, and a more in-depth exploration of XFOIL will provide a better understanding of its limitations and capabilities. Using both solvers in tandem for specific Mach-alpha combinations can improve efficiency in generating airfoil tables.

ACKNOWLEDGMENTS

REFERENCES

1. Anderson, J.D., *Fundamentals of aerodynamics*, 5th Ed., McGraw Hill, 2007.
2. Abbott, I.H., Von Doenhoff, A.E., *Theory of Wing Sections*, Dover Publications, New York, New York, 1959.
3. McCroskey, W.J, "A Critical Assessment of Wind Tunnel Results for the NACA 0012 Airfoil," NASA/TM-100019, 1987.
4. Harris, C. D. "Two-Dimensional Aerodynamic Characteristics of the NACA 0012 Airfoil in the Langley 8 Foot Transonic Pressure Tunnel," NASA Technical Memorandum 81927, 1981.
5. Davis, J.M., "Rotorcraft Flight Simulation with Aeroelastic Rotor and Improved Aerodynamic Representation, Volume II User's Manual," Bell Helicopter Company, AD-782 756, 1974.
6. Noonan, K.W., Bingham, G.J., "Aerodynamic Characteristics of Three Helicopter Rotor Airfoil Sections at Reynolds Number from Model Scale to Full Scale at Mach Numbers from 0.35 to 0.90," NASA TP-1701, 1980.
7. Flemming, R. J., "An Experimental Evaluation of Advanced Rotorcraft Airfoils in the NASA Ames

Eleven-Foot Transonic Wind Tunnel," NASA/CR-166587, 1984.

8. Sukra Helitek, Inc. "OVERFLOW Module for AFTGen Application User Manual," Ames, Iowa. 26 June 2020.

9. Drela, M., "XFOIL: An Analysis and Design System for Low Reynolds Number Airfoils," Low Reynolds Number Aerodynamics. p. 12, 1989.

10. Nichols, R., Buning, P., "User's Manual for OVERFLOW 2.3", NASA Langley Research Center. February 2021.

11. UIUC Airfoil Data Site. 2022. UIUC Airfoil Coordinates Database. [online] Available at: https://m-selig.ae.illinois.edu/ads/coord_database.html

12. Anderson, J.D., *Introduction to Flight*, 3rd Edition, McGraw Hill, 1989.